Effect of sampling time in the laboratory investigation of braided rivers

AGU PUBLICATIONS

Water Resources Research

TECHNICAL REPORTS: METHODS

10.1002/2017WR020474

**Key Points:**
- We show an experimental technique that allows flume transects profiling with a sampling frequency of 4 min without stopping the water flow
- The technique is used to continuously acquire the topography of a transect in 12 braided rivers with different experimental conditions
- The precision of the topography measurement depends on the survey frequency and on the river dimensionless stream power

**Supporting Information:**
- Supporting Information S1

**Correspondence to:**
R. Vesipa,
riccardo.vesipa@polito.it

**Citation:**
Vesipa, R., and C. Camporeale (2017), Effect of sampling time in the laboratory investigation of braided rivers, *Water Resour. Res.*, *53*, doi:10.1002/2017WR020474.

Received 24 JAN 2017
Accepted 3 JUN 2017
Accepted article online 9 JUN 2017



# Effect of sampling time in the laboratory investigation of braided rivers

**R. Vesipa[1], C. Camporeale[1], and L. Ridolfi[1]**

[1]Department of Environment, Land and Infrastructure Engineering, Politecnico di Torino, Torino, Italy

**Abstract** We focus on the measurement of the bed-elevation of braided networks in flume experiments. In particular, the effect of the survey frequency on the measurement accuracy is studied. To this aim, an innovative measurement system is adopted. It consists of a laser-ultrasonic sensor and can survey the bed-elevation under flowing water. This measurement system was used to profile a flume transect with a frequency of 4 min, without stopping the water discharge. By this technique, the topography of a single transect was continuously acquired during the evolution of a braided river model. Twelve braided rivers generated with different experimental conditions were studied. The main results are (i) there exists a threshold survey frequency (4–8 min in our analysis) which guarantees that the morphological evolution of the braiding channels is fully measured; (ii) if this threshold frequency of survey is exceeded, significant errors occur in the balance of the eroded/deposited sediments and in the evaluation of the bed-elevation dynamics; and (iii) these errors depend on the river stream power.

## 1. Introduction

Braided rivers are complex fluvial systems. They are originated by morphological processes that trigger recurring flow divergences and convergences [*Ashmore*, 1991; *Ashworth*, 1996; *Bertoldi*, 2012; *Federici and Paola*, 2003]. These processes generate floodplains characterized by a great number of islands separated by multiple branches [*Murray and Paola*, 1994; *Van Der Nat et al*., 2003; *Bertoldi et al*., 2009a; *Ashmore*, 2013]. A key characteristic of the braided patterns is the coexistence of several morphological mechanisms that act at very different spatial and temporal scales. The interaction of these mechanisms induces strong fluctuations in time and space of the bed-elevation [*Hicks et al*., 2007; *Milan et al*., 2007; *Bertoldi et al*., 2009a; *Ashmore et al*., 2011].

The knowledge of braiding dynamics is crucial in many fields, ranging from ecology [*Richards et al*., 2002; *Beschta and Ripple*, 2012; *Bertoldi et al*., 2015; *East et al*., 2016] to engineering [*Bristow and Best*, 1993; *Roach et al*., 2005; *Jang and Shimizu*, 2007; *Piégay et al*., 2009] and river restoration [*Rohde et al*., 2004; *Jaquette et al*., 2005; *Jähnig et al*., 2009; *East et al*., 2015]. The first studies about braiding focused on unveiling the key physical mechanisms that generate braided patterns [*Ashmore*, 1982; *Ashmore and Parker*, 1983; *Ashmore*, 1991, 1993]. Nowadays, the research is more oriented to quantify the processes that drive braided systems [*Bertoldi and Tubino*, 2005; *Bertoldi et al*., 2009a; *Egozi and Ashmore*, 2008; *Bertoldi et al*., 2009b]. In this scenario, the measurement of bed-elevation is fundamental in a number of issues. Examples are the evaluation of the sediment discharge [*Martin and Church*, 1995; *McLean et al*., 1999; *Milan et al*., 2007; *Anderson and Pitlick*, 2014] and of the shear stresses [*Paola*, 1996; *Nicholas*, 2000], the study of the effect of vegetation on the geomorphological evolution of rivers [*Gran and Paola*, 2001; *Tal and Paola*, 2007; *Bertoldi et al*., 2011; *Vesipa et al*., 2015], and the definition of indicators for the assessment of the morphological status of rivers [*Mosley*, 1982; *Redolfi et al*., 2016].

The measurement of the bed-elevation in braided patterns is a difficult task, not yet fully addressed. Three main problems hinder a precise and frequent survey of bed-elevation [*Williams et al*., 2014]. The first (morphological) problem [*Lane*, 2000; *Brasington et al*., 2003; *Casas et al*., 2010; *Wheaton et al*., 2010] is related to the steep gradient occurring in braided patterns (e.g., island edges). The second (wetted channel) problem [*Brasington et al*., 2000; *Fuller et al*., 2003; *Westaway et al*., 2003] concerns the acquisition of the topography below the water surface. Finally, the third (mobility) problem [*Lindsay and Ashmore*, 2002; *Milan et al*., 2007] is associated with the fast reworking of the bed morphology. The mobility and the wetted channel

problems are the toughest to face, in order to obtain meaningful measurements of the bed-elevation. In fact, changes of the bed-elevation mainly occur very quickly during high water stages. However, during these high stages, bed-elevation surveys are very difficult for technical reasons (e.g., turbidity, wood debris, and high velocity of the current). It follows that most of the current quantitative knowledge about braiding dynamics is based on the measurement of the fixed morphologies that emerge at low water stages. Hence, little data about the evolution that occurs between these fixed morphology are available. In this scenario, a remarkable exception is the work by *Williams et al*. [2015]. They developed an approach for the field survey of the morphological evolution of the bed during high flows.

*Lindsay and Ashmore* [2002] pointed out this issue for the first time. They studied the flume model of a braiding river. The river model was flooded by pulses of high water stages that lasted 10 min. The bed topography was surveyed by photogrammetry during the dry periods between the high water stages, and a digital elevation model (DEM) of the flume was obtained. Erosion and deposition volumes were evaluated as the difference of DEMs. It was found that the coarsening of the survey frequency induced a strong bias in the evaluation of the eroded/deposited volumes (up to 400%). A similar experiment was repeated on the field by *Milan et al*. [2007] and led to similar results.

These seminal studies revealed that the bed-elevation of braided patterns is reworked with very short time scales. However, some questions remained open. In particular, *Lindsay and Ashmore* [2002] could not reduce the duration of the formative pulses below 10 min. Hence, the occurrence of significant morphological processes acting with a time scale below 10 min was not ruled out. Moreover, the role of the experimental conditions (e.g., slope and water discharge) was not investigated.

The purpose of this work is to present an experimental technique that can answer the open issues previously discussed. To this aim, we used an experimental apparatus (section 2.1) affected to a minor extent by the three problem highlighted by *Williams et al*. [2014]. In particular, (i) the apparatus measures with very high resolution along the transect (3 points/mm), (ii) it measures underwater bed surfaces without requiring the water discharge to be stopped, and (iii) it provides the profile of a river transect with a high frequency (sampling time is 4 min). This apparatus was adopted to continuously survey the topography of a single transect. In each run, the data acquisition lasted for tens of hours (see section 2.2) and 12 braided patterns generated with different experimental conditions were surveyed (section 2.3).

The analysis of the collected data (section 3) showed that (i) the survey of a transect with a sampling time of 4 min captures all the relevant morphological processes which occur at the lab-scale. According to the Nyquist rule, the highest frequency in the braiding dynamics is of the orders of 1/8 $\text{min}^{-1}$ $\sim 1/480$ Hz; (ii) if the surveying frequency is coarsened, strong biases in the statistical properties of the bed-elevation time series (e.g., standard deviation) arise; and finally (iii) the specific experimental conditions strongly influence the precision of the bed measurement, for a given sampling time.

## 2. Methods

### 2.1. Flume Setup

The experiments were performed in the "G. Bidone" Water Science Laboratory at Politecnico di Torino. The flume (A in Figure 1a) is 18 m long and 0.6 m deep. Two side-walls built by polycarbonate sheets (B) limit the flood plain width to 2 m. Sand with specific weight of 2650 $\text{kg/m}^3$ and mean grain size $\tilde{d}_{50}=0.45$ mm (tilde denotes dimensional quantities) was used for the experiments [see *Visconti et al*., 2010 for further details]. A water stilling tank (C) is used to supply the prescribed water discharge. Another tank (D) collects the water and the sediments at the flume end. A moving weir (E) regulates the downstream water level during the experiments, while a siphon (F) removes the sand collected in the tank D. The water discharged in C is regulated by a computerized flow-control-valve (G). Finally, a mechanical hopper (H) equipped with a computer-controlled vibrating panel supplies the upstream bed load.

A key additional equipment is a three-axis CNC (computer numerical controlled) gantry (I). It carries a scraper and the measurement system (MS) for profiling flume cross sections while water is flowing. The origin of the reference system $\{\tilde{x},\tilde{y},\tilde{z}\}$ (point O in Figure 1b) is set on the middle of the CNC gantry. The position of the gantry is in the middle of the flume, thus the coordinate $\tilde{y}=9$ m refers to the flume inlet and $\tilde{y}=-9$ m to the flume outlet. The gantry can be moved along the $\tilde{y}$ axis. The sand scraper (Figure 1c) can

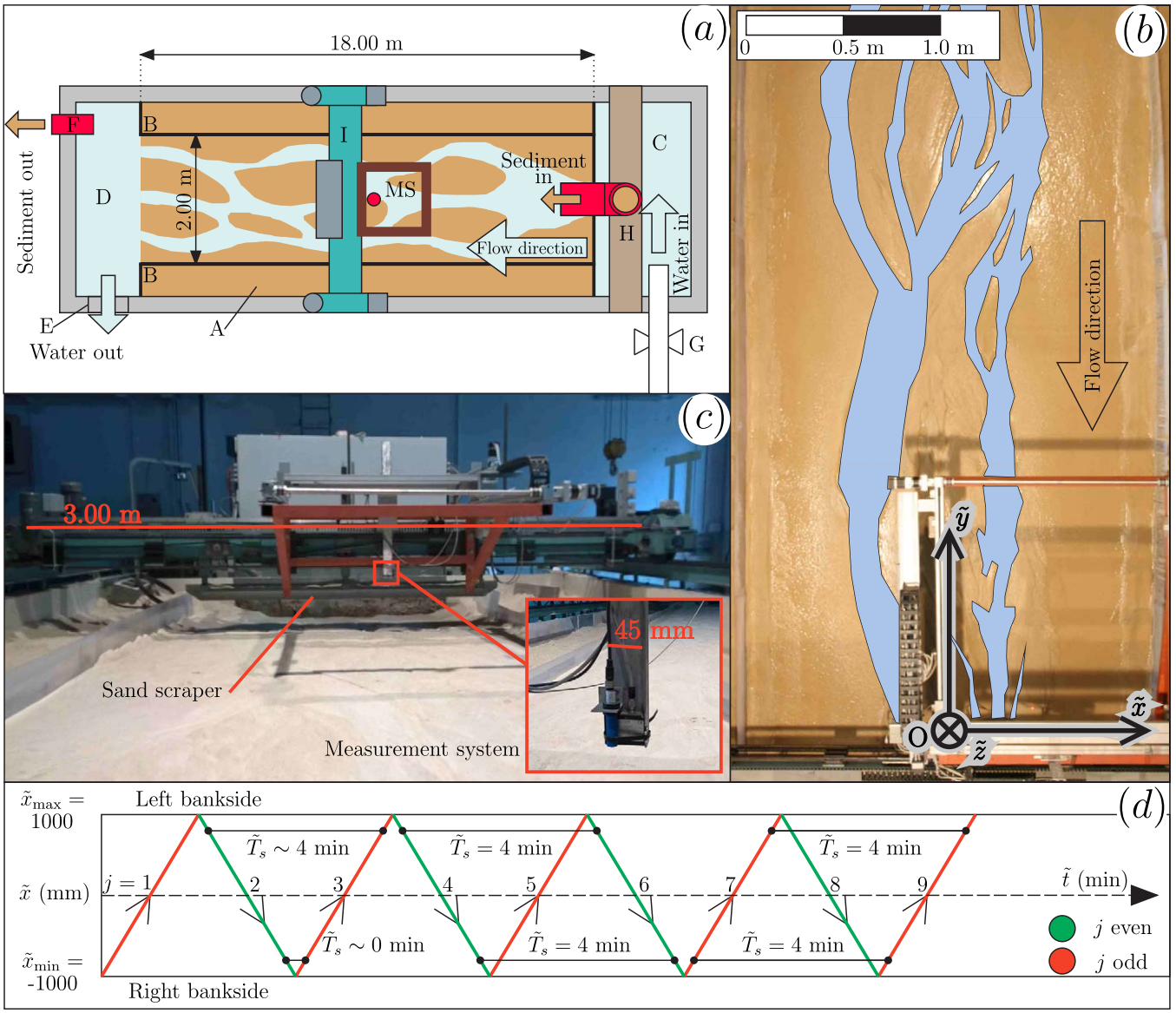


**Figure 1.** (a) Scheme of the laboratory flume. (b) Close-up of the gantry and reference system. (c) Picture of the gantry. (d) Spatiotemporal trajectory of the position of the MS. In order to profile the transect, the MS repeatedly scans the bed-elevation from $\tilde{x}_{min}$ to $\tilde{x}_{max}$ (red) and in the reverse direction (green).

be lifted along the $\tilde{z}$ axis to grade the initial channel and floodplain configuration and slope. Finally, the MS can be translated along $\tilde{x}$ with a precision of $\pm$0.5 mm.

### 2.2. Profiling of the Flume Cross Section

During the runs, the bed-elevation of the cross section $\tilde{y}$=0 was repeatedly surveyed using a nonintrusive measurement system (MS) designed by two of the authors. The MS consists of one laser triangulator and one ultrasonic sensor and can profile the bed under flowing water. A detailed description and validation of the MS is available in *Visconti et al.* [2012], whereas its key characteristics are briefly recalled in the supporting information.

The adopted MS measures the distance between the sensors and the target bed surface, $\tilde{H}$, in a fixed point. Hence, the translation of the MS from one bank-side to the opposite bank-side provides the river transect profile of $\tilde{H}$. This translation is performed in $\tilde{T}_t$=2 min, in order to minimize mechanical vibrations and to measure $\tilde{H}$ with a spatial resolution of 3 points/mm. In Figure 1d, the spatiotemporal trajectory of the MS is sketched. It is apparent that the continuous evolution of the bed-MS distance $\tilde{H}(\tilde{x},\tilde{t})$ is acquired by the MS

as a discrete set of transect profiles. The $j$th profile is denoted as $\tilde{H}_j(\tilde{x})$, where $j$ is an integer number. When $j$ is odd, the MS acquires the profile translating from $\tilde{x}=-1000$ mm to $\tilde{x}=1000$ mm (red in Figure 1d). When $j$ is even the acquisition is done in the reverse direction (green). It follows that the time interval $\tilde{T}_s$ between the acquisition of $\tilde{H}$ in the profile $j$ and in the profile $j+1$ is not constant along the transect. Indeed, it depends on $\tilde{x}$ (e.g., see profiles 2–3 in Figure 1d). Differently, the sampling time between the profile $j$ and the profile $j+2$ (or multiple) is constant throughout the profile (e.g., profiles 4–6 or 7–9). Therefore, the profiles $\tilde{H}_j$ are divided in two data sets. The data set $\tilde{H}_{j,odd}$ ($\tilde{H}_{j,even}$) is made up of profiles with $j$ odd (even) only. This ensures a constant sampling time between profiles of the same data set, at any $\tilde{x}$. It should also be noted that the $j$th profile is acquired in the time interval $[(j-1)\tilde{T}_t, j\tilde{T}_t]$. In the following, it is conventionally assumed that the profile is instantaneously measured at the time $\tilde{t}_j=j\tilde{T}_t$.

We focused on braided networks in statistical equilibrium. To this aim, we considered only the profiles acquired after $\tilde{t}=\tilde{T}_{eq}$ from the beginning of the run, where $\tilde{T}_{eq}$ is the minimum duration of the run that guarantees that the condition of statistical equilibrium is reached in the braided pattern. According to *Bertoldi et al*. [2009a,b] we set $\tilde{T}_{eq}=1000$ min for all runs. From a practical viewpoint, we set $\tilde{t}=0$ and $j=1$ after the time interval $\tilde{T}_{eq}$ was passed from the beginning of the run.

The bed-elevation of the transect at a generic $\tilde{t}=\tilde{t}_j$ when $j$ is odd reads

$$\tilde{\eta}_{j,odd}(\tilde{x})=\tilde{H}_{odd,0}-\tilde{H}_{j,odd}(\tilde{x}), \tag{1}$$

where $\tilde{H}_{odd,0}$ is a reference distance between the bed and the MS. It is evaluated as

$$\tilde{H}_{odd,0}=\frac{1}{N_{odd}}\sum_{j=1}^{N}\langle\tilde{H}_{j,odd}(\tilde{x})\rangle \quad (j\,\text{odd}), \tag{2}$$

where $N_{odd}$ is the number of odd profiles, and $\langle\cdot\rangle=\int_{\tilde{x}_{min}}^{\tilde{x}_{max}}\cdot/(\tilde{x}_{max}-\tilde{x}_{min})\mathrm{d}\tilde{x}$ denotes the spatial average along the transect. Hence, $H_{odd,0}$ is the spatiotemporal average of the odd profiles measured in statistical-equilibrium conditions. Figure 2a reports an example of the bed topography dynamics obtained plotting $\tilde{\eta}_{j,odd}$ in space and time. The data set $\tilde{\eta}_{j,even}$ was built with an analogous procedure, but considering $j$ even. All the results presented in the following sections were obtained analyzing the data sets $\tilde{\eta}_{j,even}$ and $\tilde{\eta}_{j,odd}$ separately, and then averaging the corresponding outcomes. The differences between the two data sets were always very small. For this reason and for the sake of simplicity, in section 3, the term $\tilde{\eta}_j$ refers to $\tilde{\eta}_{j,even}$ or $\tilde{\eta}_{j,odd}$, indifferently.

### 2.3. Runs

In order to generate a braided river morphology, the scraper was first used to grade a floodplain with slope $S$ that accommodated a straight 0.50 m wide rectangular channel. The channel depth, $\tilde{Z}$, was chosen to ensure bankfull conditions with the prescribed water discharge $\tilde{Q}$ [*Ashmore*, 1991; *Bertoldi et al*., 2009a]. Second, the run was started by supplying the liquid discharge $\tilde{Q}$ and the solid discharge $\tilde{Q}_s$, where this latter term was calculated by using the results of *Bertoldi et al*. [2009b]. Third, at the end of each run, all the sand collected in the tank D was dried and weighted. The weight of the sand discharged by the mechanical hopper (H in Figure 1) was compared with the weight of the sand collected in the downstream tank (D). A very good match was found between incoming and outgoing sediments in all runs (maximum relative error below $\pm5\%$). This means that the mean elevation of the whole flume was constant and no aggradation or degradation processes occurred.

Twelve braided streams were generated in the flume, in order to explore different experimental conditions. The experimental characteristics of each run are summarized in Table 1. In order to determine the experimental conditions, the channel width $\tilde{W}$, the floodplain slope $S$, and the liquid discharge $\tilde{Q}$ were first set. The solid discharge $\tilde{Q}_s$ and the channel height $\tilde{Z}$ were then evaluated to meet the requirement of bed-elevation equilibrium and to have bankfull conditions in the rectangular channel, respectively.

To characterize the runs from an hydraulic and morphodynamic viewpoint, the Froude number, $Fr$, the aspect ratio, $\beta$, the Shields stress, $\Theta$, the dimensionless flow rate, $q$, and the dimensionless stream power, $\omega$, were evaluated as

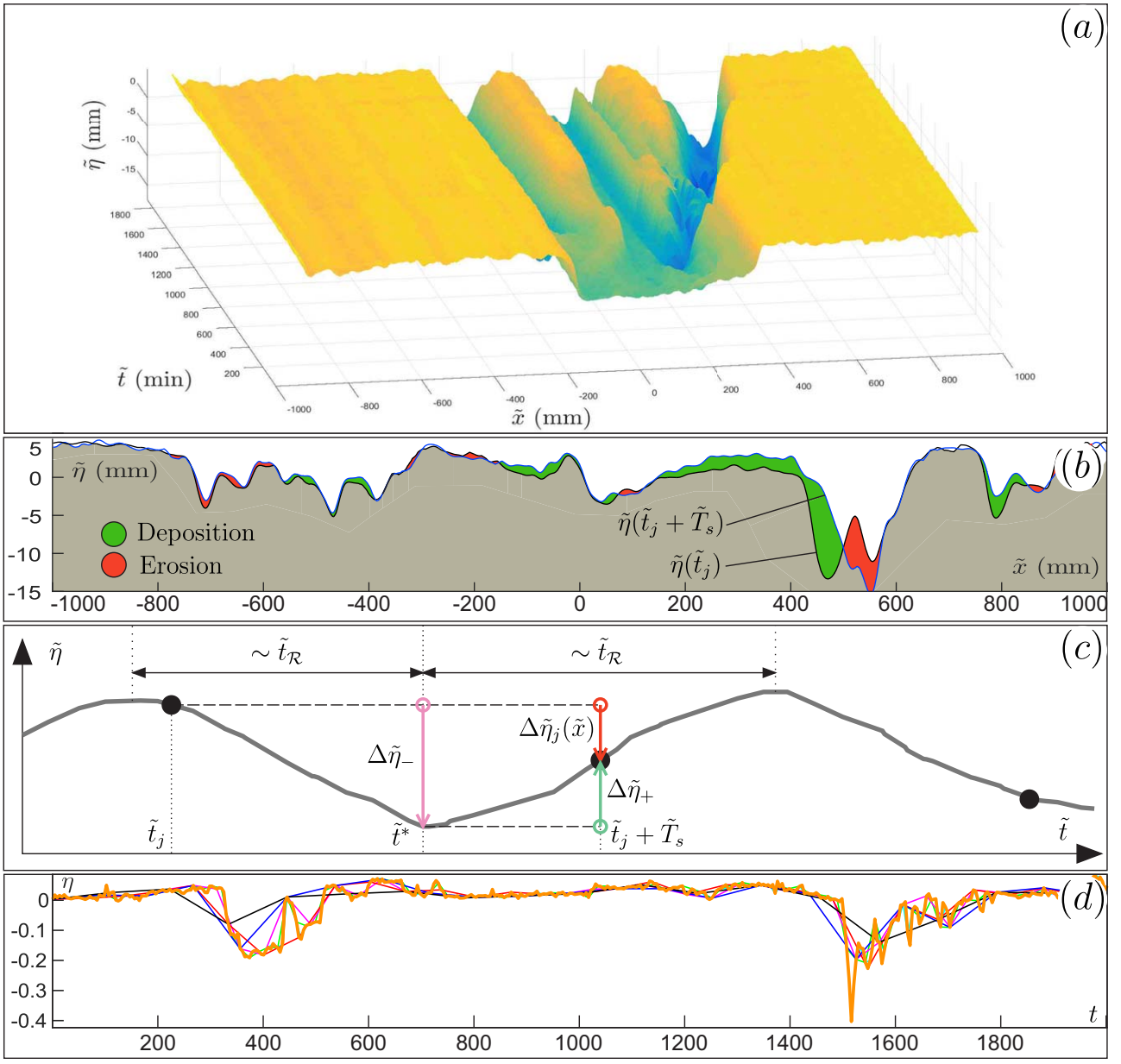


**Figure 2.** (a) Example of the surface $\tilde{\eta}(\tilde{x}, \tilde{t}_j)$ during run 1, at $\tilde{y}=0$, obtained from the data set $\tilde{\eta}_{j,odd}$. For $\tilde{t} \sim 0$ the flume cross section is the rectangular channel carved by the scraper. (b) Example of the temporal evolution of a profile $\tilde{\eta}$ from $\tilde{t}_j$ to $\tilde{t}_j+\tilde{T}_s$ (run 6). (c) Exemplifying sketch of the bed-elevation in a fixed plot $\tilde{x}$. The black line is the continuous real time-evolution of the bed-elevation in the plot. The dots are the discrete values of $\tilde{\eta}$ that are sampled by the measurement system at the times $\tilde{t}_j$ with sampling time $\tilde{T}_s$. (d) Example of the bed-elevation dynamics at the plot $x = 0$, namely $\eta(x=0, t_j, T_s)$ in the run 6. Different curves refer to different $T_s$ (see the legend in Figure 3 for the color meaning).

$$Fr=\frac{\tilde{Q}}{\tilde{W}\sqrt{g\tilde{D}_0^3}},\ \beta=\frac{\tilde{W}}{\tilde{D}_0},\ \Theta=\frac{\tilde{\tau}}{(\rho_s-\rho)g\tilde{d}_{50}},\ q=\frac{\tilde{Q}}{\mathcal{L}\sqrt{\Delta g\tilde{d}_{50}^3}},\ \omega=q\cdot S, \tag{3a-3e}$$

where $\tilde{D}_0=\tilde{Z}$ is the water depth, $\tilde{\tau}$ is the average bed shear stress, $\rho_s$ and $\rho$ are the sediment and water densities, $g$ is gravity, and $\Delta=(\rho_s-\rho)/\rho$. The length scale $\mathcal{L}=\tilde{Q}^{2/5}/g^{(1/5)}$ was introduced by *Parker et al.* [2007] and is usually adopted to normalize morphometric quantities in braided rivers [*Bertoldi et al.*, 2009a]. Additionally, we introduced the temporal scale $\mathcal{T}=\mathcal{L}^2/\sqrt{\Delta g\tilde{d}_{50}^3}$, so that a generic dimensional length $\tilde{l}$ or time $\tilde{t}$ was made dimensionless as

**Table 1.** Experimental Conditions of Each Run[a]

| Run | $\tilde{Q}$ (L s$^{-1}$) | $S$ (%) | $\tilde{Q}_s$ (g s$^{-1}$) | $\tilde{Z}$ (mm) | $Fr$ | $\beta$ | $\Theta$ | $\mathcal{L}$ (mm) | $q$ | $\omega$ |
|---|---|---|---|---|---|---|---|---|---|---|
| 1 | 0.7 | 0.5 | 0.30 | 7 | 0.75 | 71 | 0.048 | 35 | 493 | 2.5 |
| 2 | 1 | 0.5 | 0.44 | 9 | 0.78 | 57 | 0.059 | 40 | 610 | 3.1 |
| 3 | 1.5 | 0.5 | 1.05 | 11 | 0.81 | 45 | 0.075 | 47 | 779 | 3.9 |
| 4 | 0.7 | 1.0 | 1.06 | 6 | 1.03 | 87 | 0.077 | 35 | 493 | 4.9 |
| 5a | 1 | 1.0 | 1.74 | 7 | 1.07 | 70 | 0.096 | 40 | 610 | 6.1 |
| 5b | 1 | 1.0 | 1.74 | 7 | 1.07 | 70 | 0.096 | 40 | 610 | 6.1 |
| 5c | 1 | 1.0 | 1.74 | 7 | 1.07 | 70 | 0.096 | 40 | 610 | 6.1 |
| 5d | 1 | 1.0 | 1.74 | 7 | 1.07 | 70 | 0.096 | 40 | 610 | 6.1 |
| 6 | 1.5 | 1.0 | 2.71 | 9 | 1.11 | 55 | 0.122 | 47 | 779 | 7.8 |
| 7 | 0.7 | 1.5 | 2.12 | 5 | 1.24 | 98 | 0.103 | 35 | 493 | 7.4 |
| 8 | 1 | 1.5 | 2.72 | 6 | 1.28 | 80 | 0.127 | 40 | 610 | 9.2 |
| 9 | 1.5 | 1.5 | 6.47 | 8 | 1.33 | 62 | 0.162 | 47 | 779 | 11.7 |
| 10 | 1.5 | 1.2 | n.r. | n.r. | n.r. | n.r. | n.r. | 47 | 428 | 6.4 |

[a]Run 10 refers to the experiment performed by *Lindsay and Ashmore* [2002] and n.r. means "not reported."

$$I=\frac{\tilde{I}}{\mathcal{L}},\ t=\frac{\tilde{t}}{\mathcal{T}}. \tag{4a, 4b}$$

The parameters of equations (3) were computed with reference to the initial rectangular channel and are very similar to the experimental conditions adopted in most of the flume studies about braided rivers [e.g., *Lindsay and Ashmore*, 2002; *Bertoldi et al*., 2009a].

In order to characterize the braiding intensity, two braiding indexes were evaluated for each run: (i) the Total Braiding Index (TBI), i.e., the number of wet channels in the cross section and (ii) the Active Braiding Index (ABI), namely the number of channels that transport sediments. The procedure adopted to evaluate these indexes is reported in the supporting information. In the performed runs, the TBI ranged between 5 and 9, whereas ABI was in the range [1.5–6].

## 3. Results

### 3.1. Erosion and Deposition Dynamics

Our first focus is on the effect of the sampling time on erosion and deposition dynamics occurring at the transect scale. Figure 2b shows two typical transects acquired by the measurement system. It can be observed that the profile $\tilde{\eta}_j$ acquired at $\tilde{t}_j$ is different from the profile measured at $\tilde{t}_j+\tilde{T}_s$, and the difference between these two profiles is $\Delta\tilde{\eta}_j(\tilde{x},\tilde{T}_s)=\tilde{\eta}(\tilde{x},\tilde{t}_j+\tilde{T}_s)-\tilde{\eta}(\tilde{x},\tilde{t}_j)$. In some areas (red), erosion processes occurred ($\Delta\tilde{\eta}<0$), whereas in some others (green) deposition took place ($\Delta\tilde{\eta}>0$).

Let us first focus on erosion. The total area eroded throughout the transect during the time interval $[\tilde{t}_j,\tilde{t}_j+\tilde{T}_s]$ reads

$$\mathcal{E}(\tilde{t}_j,\tilde{T}_s)=\int_{\tilde{x}_{\min}}^{\tilde{x}_{\max}}\theta(\tilde{x},\tilde{T}_s)\frac{|\Delta\tilde{\eta}_j(\tilde{x},\tilde{T}_s)|}{\mathcal{L}^2}\mathrm{d}\tilde{x},\ \ \theta(\tilde{x},\tilde{T}_s)=\begin{cases}1 & \text{if } \Delta\tilde{\eta}_j(\tilde{x},\tilde{T}_s)\le-\tilde{\delta}\\ 0 & \text{if } \Delta\tilde{\eta}_j(\tilde{x},\tilde{T}_s)>-\tilde{\delta}.\end{cases} \tag{5}$$

It should be noted that (i) the spatial scale $\mathcal{L}^2$ is introduced to make the infinitesimal area $|\Delta\tilde{\eta}|\mathrm{d}\tilde{x}$ dimensionless and (ii) the piecewise term $\theta$ is introduced to consider in the integral only bed-elevation changes that are above the instrument precision, $\tilde{\delta}$ (according to *Lindsay and Ashmore* [2002]). Preliminary analyses estimated that the precision of the MS is $\tilde{\delta}=0.5$ mm, that is of the same order of the mean grain diameter of the sediment bed, $\tilde{d}_{50}$. The assessment of the MS precision is crucial. In fact, if the measurement system cannot detect changes below a certain resolution, more frequent surveys deliver no new information. A detailed discussion about this point, and about the role of bed roughness in defining the useful precision of the MS is reported in the supporting information.

The key point of our work is that the estimation of $\mathcal{E}$ strongly depends on the sampling time $\tilde{T}_s$ adopted in the measurement technique. In fact, "compensation" may occur between erosion and deposition processes [*Lindsay and Ashmore*, 2002]. To understand the meaning of compensation, let us consider the illustrative temporal evolution of the bed-elevation reported in Figure 2c, which refers to a generic plot $\tilde{x}$. The black

line refers to the real continuous time-evolution of the bed-elevation. The bed-elevation alternates erosion and deposition phases with typical time scale $\tilde{t}_{\mathcal{R}}$ (Figure 2c). This temporal scale is defined as "time scale of reworking." During the generic time interval $[\tilde{t}_j, \tilde{t}^*]$, the bed undergoes exclusively erosion, and the elevation reduces of $\Delta\tilde{\eta}_-$ (pink arrow in Figure 2c). On the other hand, when $\tilde{t} \in [\tilde{t}^*, \tilde{t}_j+\tilde{T}_s]$, only deposition takes place and the elevation increases of $\Delta\tilde{\eta}_+$ (green arrow). Let us consider now the discrete measurement of $\tilde{\eta}$ performed with sampling time $\tilde{T}_s$ (black dots in Figure 2c). If $\tilde{\eta}$ is measured at $\tilde{t}_j$ and at $\tilde{t}_j+\tilde{T}_s$, the estimated bed-elevation-alteration is $\Delta\tilde{\eta}_j(\tilde{x})=\Delta\tilde{\eta}_-+\Delta\tilde{\eta}_+$ (red arrow in Figure 2c). This estimated erosion is lower than the erosion $\tilde{\eta}_-$ actually experienced by the bed. In fact, the deposition $\Delta\tilde{\eta}_+$ has partially compensated the erosion. Thus, the eroded area $\mathcal{E}$ can be strongly underestimated, if $\tilde{T}_s$ is much greater than the typical time scale of reworking $\tilde{t}_{\mathcal{R}}$.

The eroded area in the transect during the sampling interval $[\tilde{t}_j, \tilde{t}_j+\tilde{T}_s]$ (i.e., $\mathcal{E}$ in equation (5)) is used to evaluate the two key metrics

$$E(t_j, T_s)=\sum_{i=1}^{j}\mathcal{E}(\tilde{t}_i, \tilde{T}_s), \quad e(t_j, T_s)=\frac{\mathcal{E}(\tilde{t}_j, \tilde{T}_s)}{\tilde{T}_s}, \tag{6a, 6b}$$

where $E(t_j, T_s)$ is the cumulative area eroded from $\tilde{t}=0$ to $\tilde{t}=\tilde{t}_j$, whereas $e(t_j, T_s)$ is the instantaneous rate of erosion. In order to evaluate $E(t_j, T_s)$ and $e(t_j, T_s)$ from $\mathcal{E}(\tilde{t}_j, \tilde{T}_s)$, the dimensional sampling time $\tilde{T}_s$ was replaced with its dimensionless counterpart $T_s=\tilde{T}_s/\tilde{T}_{s,\min}$, where $\tilde{T}_{s,\min}=4$ min. This was done to better highlight the effects of the increment of the sampling time. It should be noted that the time during which the transect profile is acquired was evaluated in dimensionless terms as $t_j=\tilde{t}_j/\mathcal{T}$.

If the same rationale is applied to deposition processes, it is possible to define the cumulative area deposited in the whole transect, $D(t_j, T_s)$, and the instantaneous rate of deposition, $d(t_j, T_s)$. Finally, to quantify the total morphological activity, the cumulative reworked area $R(t_j, T_s)=E(t_j, T_s)+D(t_j, T_s)$ and the reworking rate $r(t_j, T_s)=e(t_j, T_s)+d(t_j, T_s)$ are defined.

In Figure 3, the results of our experimental work are shown. Figure 3a reports the cumulative reworked area $R(t_j)$ evaluated with different sampling times, for the exemplifying run 6. It can be observed that while $T_s$ increased, $R(t_j)$ decreased. At the end of the run, the cumulative reworked area evaluated with $T_s=1$ (i.e., $\tilde{T}_s=4$ min) was almost 4 times the area evaluated with $T_s=25$ ($\tilde{T}_s=100$ min). Moreover, the curves evaluated with $\tilde{T}_s=4$ min and with $\tilde{T}_s=8$ min basically coincide. This demonstrates that the typical reworking time scale in our experiments is about 4–8 min. In other words, in a generic plot, the bed-elevation underwent exclusively erosion or exclusively deposition for periods of about 4–8 min. For a sampling time shorter than 8 min, compensation did not occur and the curves $R(t_j, 1)$ $(\tilde{T}_s=4\,\text{min})$ and $R(t_j, 2)$ $(\tilde{T}_s=8\,\text{min})$ match. In other runs, the curves are always very close, even though they sometimes do not match perfectly. In contrast, for sampling times longer than 8 min, compensation occurred, and the estimation of the cumulated reworked area was significantly reduced. This result is consistent and fills a gap in the sample set of the work by *Lindsay and Ashmore* [2002]. They used experimental conditions comparable with run 6 (see Table 1) and found that erosion and deposition volumes evaluated with $\tilde{T}_s=10$ min are 420% higher than those evaluated with $\tilde{T}_s=100$ min. However, the case $\tilde{T}_s<10$ min had not been investigated. Therefore, the occurrence of compensation during the time interval $\tilde{T}_s=10$ could not be definitively ruled out. It should be noted that the curves $R(t_j)$ are significantly influenced by the instrument precision $\tilde{\delta}$. A sensitivity analysis with respect to $\tilde{\delta}$ is reported in the supporting information.

Figures 3b–3d extend the analysis to the instantaneous rate of reworking. Figure 3b reports the time series $r(t_j)$ and Figure 3c shows the cumulative distribution functions (CDF) of $r(t_j)$. Finally, the frequency-spectra of $r(t_j)$ are given in Figure 3d. Two key behaviors stand out in Figure 3b. First, the lower the sampling time, the higher the measured reworking rate. This is also well visible comparing the yellow and the magenta CDFs in Figure 3c. When $\tilde{T}_s=4$ min (yellow) the reworking rate exhibits a right tail till $1.2\times10^{-7}$ and, on average, $r(t_j)$ is around $0.40\times10^{-7}$ (see $P(r)=0.50$ in Figure 3c). Differently, for $\tilde{T}_s=40$ min (magenta), $r(t_j)$ does not exceed $0.4\times10^{-7}$ and, on average is $0.15\times10^{-7}$. Second, the curves $r(t_j)$ evaluated with a short $\tilde{T}_s$ show a strong temporal variability, and vice versa. This means that the lower the sampling time, the richer the spectrum of $r(t_j)$. For example, let us consider again the cases $\tilde{T}_s=4$ min and $\tilde{T}_s=40$ min in Figure 3d. In the former case (yellow), the spectrum $r(f)$ shows that frequencies up to $5\times10^{-2}$ are relevant. On the opposite, the magenta curve shows that only frequencies much below $5\times10^{-3}$ are measured.

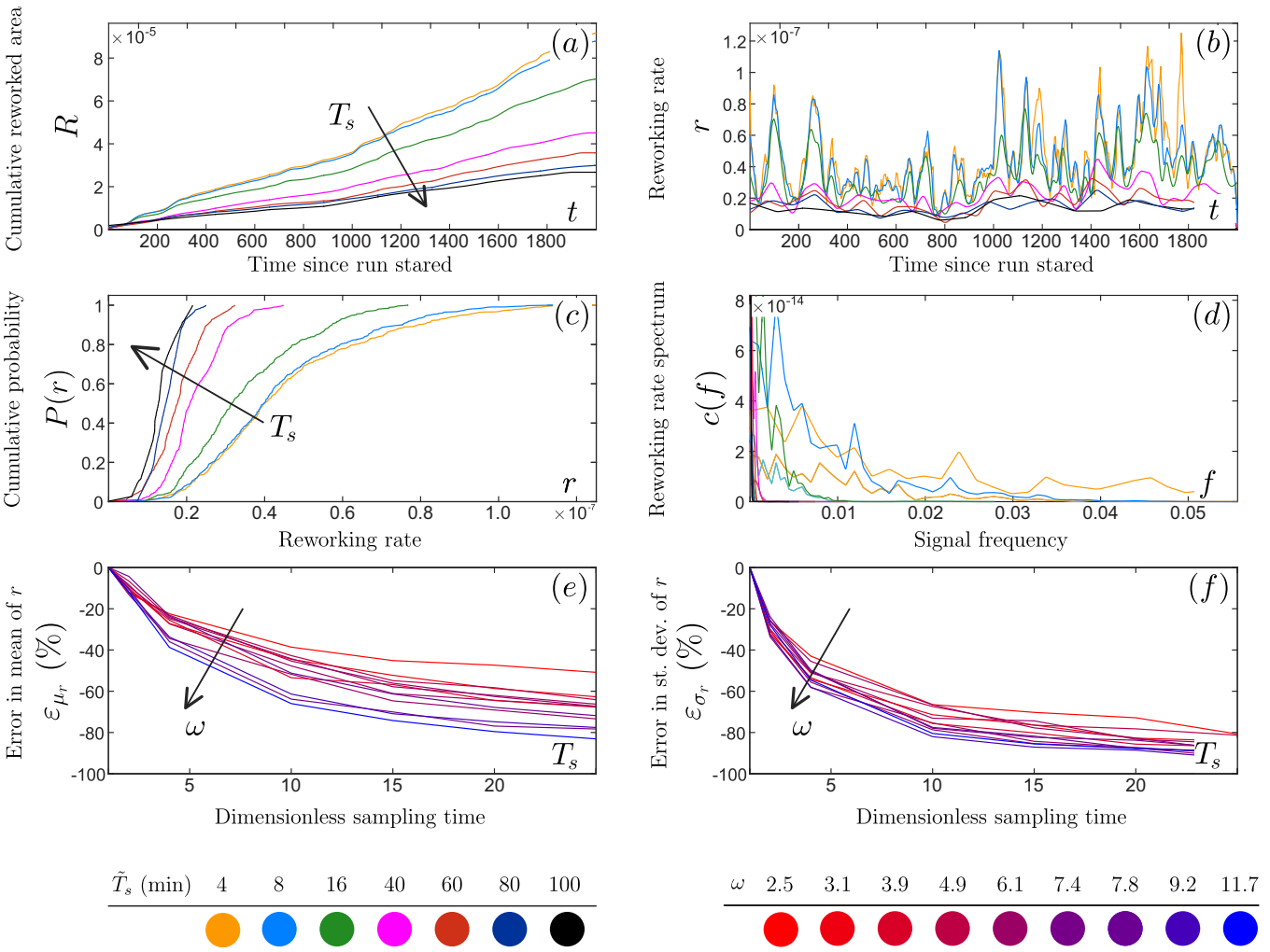


**Figure 3.** (a) Cumulative reworked area, $R(t_j, T_s)$. (b) Reworking rate, $r(t_j, T_s)$. (c) CDF of $r(t_j)$. (d) Spectrum of $r(t_j)$. (a–d) Data are from run 6 (see the supporting information for the other runs). (e, f) The $T_s$-dependent $\varepsilon_{\mu_r}$ and $\varepsilon_{\sigma_r}$ for different runs.

The effect of the experimental conditions on the error induced by the coarsening of the sampling frequency was also investigated. To facilitate the comparison of the results of different run, we first defined the $T_s$-dependent mean morphological activity, $\mu_r(T_s)=\sum_{j=1}^{N} r(t_j, T_s)/N$, and the standard deviation $\sigma_r(T_s)=\{\sum_{j=1}^{N} [r(t_j, T_s)-\mu_r]^2/N\}^{1/2}$ (we recall that $N$ is the number of profiles). The errors induced by an increment of the sampling time were evaluated with respect to the minimum sampling time case, namely

$$\varepsilon_{\mu_r}(T_s)=\frac{\mu_r(T_s)-\mu_r(T_{s,\min})}{\mu_r(T_{s,\min})},\quad \varepsilon_{\sigma_r}(T_s)=\frac{\sigma_r(T_s)-\sigma_r(T_{s,\min})}{\sigma_r(T_{s,\min})}, \tag{7a, 7b}$$

where we recall, $T_{s,\min}=1$. The variable $\varepsilon_{\mu_r}$ quantifies the error (with respect to the case $T_s=T_{s,\min}$) in the estimation of the mean reworking rate, $\mu_r$, when $T_s$ increases. Similarly, $\varepsilon_{\sigma_r}$ gives the $T_s$-dependent error in the evaluation of the temporal variability of the reworking rate. The dimensionless stream power $\omega$ was used to summarize the flow rate $\tilde{Q}$ and the bed slope $S$ in one parameter only. It was found that $\varepsilon_{\mu_r}$ and $\varepsilon_{\sigma_r}$ showed a significant correlation with $\omega$. In contrast, no consistent trend was detected if the dimensionless flow rate $q$ was used in place of $\omega$ (see the supporting information). Figures 3e and 3f report the error induced by increments of $T_s$ on the metrics $\mu_r$ and $\sigma_r$, for all the performed runs. It is apparent that the increment of $\omega$ renders the evaluation of $\mu_r$ or $\sigma_r$ more sensitive to the increment of the sampling time. For $\mu_r$ (Figure 3e), the error is smaller than $\simeq$ 50% when $\omega=2.5$ (red curve) whereas it exceeds $\simeq$ 80% when

$\omega$=11.7 (blue curve). A similar behavior is observed also for the curves $\varepsilon_{\sigma_r}$ (see Figure 3f). However, the curves show a low dispersion while the stream power $\omega$ varies. In fact, for $T_s = 25$, $\varepsilon_{\sigma_r}$ is in the narrow range 80%–90% for all the values of $\omega$.

### 3.2. Bed-Elevation Dynamics

We now focus on the effect of the sampling time, $T_s$, on the measurement of the bed-elevation. To this end, we first evaluate the $T_s$-dependent temporal evolution of the bed-elevation in a generic plot. As an example, Figure 2d shows $\eta(x{=}0, t_j, T_s)$ evaluated for different $T_s$. It is apparent that an increment of $T_s$ reduces the temporal variability of the elevation $\eta$. To quantify this reduction of variability, we evaluated the standard deviation of the bed-elevation, $\sigma_\eta(x, T_s) = \{\sum_{j=1}^{N} [\eta(x, t_j, T_s) - \mu_\eta(x, T_s)]^2 / N\}^{1/2}$, where $\mu_\eta(x, T_s) = \sum_{j=1}^{N} \eta(x, t_j, T_s)/N$ is the temporal average of bed-elevation in the $x$ plot. The metric $\sigma_\eta$ is $T_s$ and plot dependent, and an example of the dependence $\sigma_\eta = \sigma_\eta(x)$ is shown by the curve reported in Figure 4a. The curve in Figure 4a refers to $T_s = T_{s,\min} = 1$. It is used as a reference value of $\sigma_\eta(x)$ for assessing the magnitude of the error that occurs when $T_s > T_{s,\min}$. This error reads

$$\varepsilon_{\sigma_\eta}(x, T_s) = \frac{|\sigma_\eta(x, T_s) - \sigma_\eta(x, T_{s,\min})|}{\sigma_\eta(x, T_{s,\min})}. \tag{8}$$

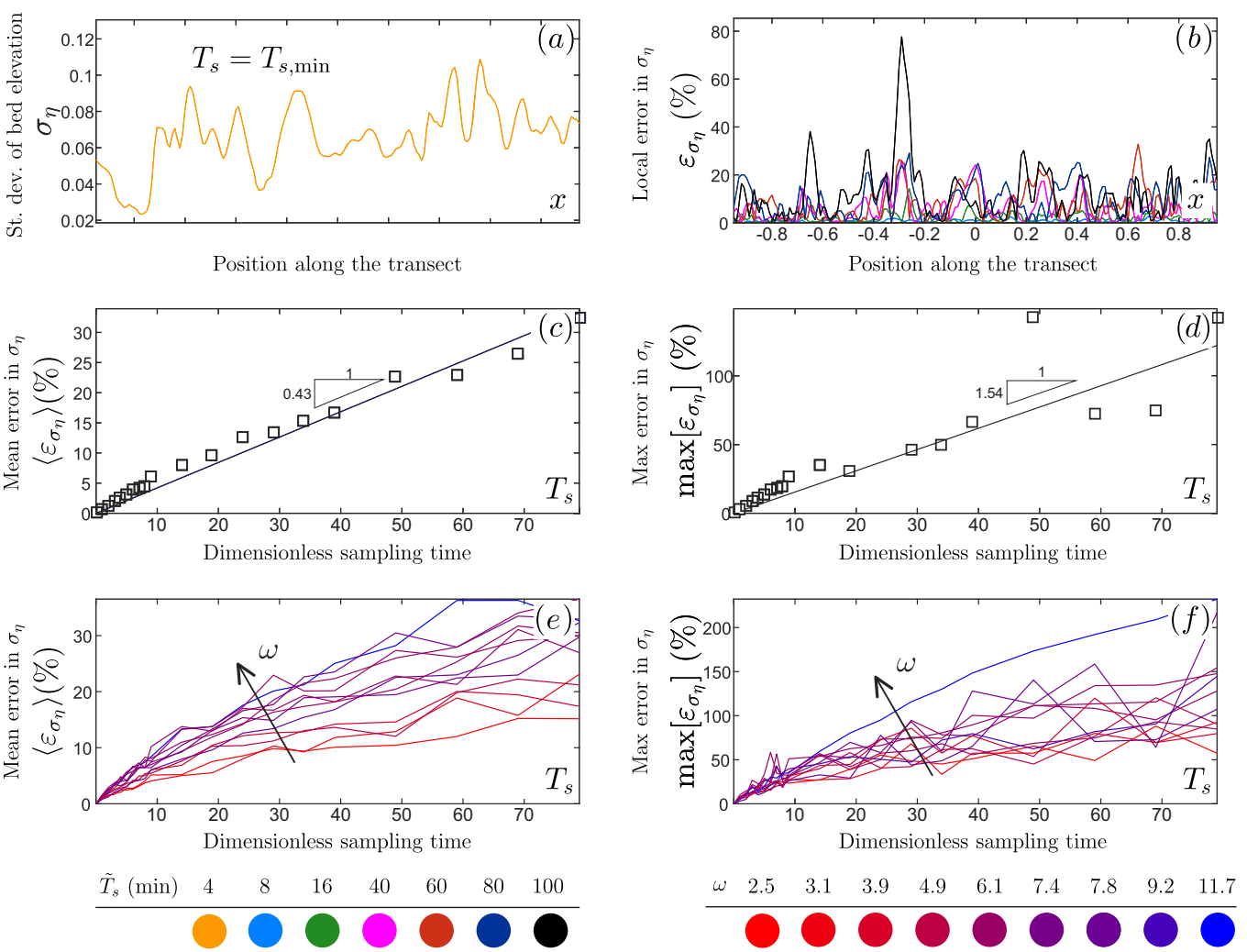


**Figure 4.** (a) $\sigma_\eta(x, T_s)$ for $T_s = T_{s,\min} = 1$. (b) $\varepsilon_{\sigma_\eta}(x)$ for different $T_s$ (different colors). ($c$–$d$) $\langle \varepsilon_{\sigma_\eta}(x) \rangle$ and max $[\varepsilon_{\sigma_\eta}(x)]$ as a function of $T_s$. The straight lines qualitatively show the trend of errors and were obtained by a least square interpolation of the data. All data in Figure 4a–4d refer to run 6 (see the supporting information for other runs). ($e$–$f$) $\langle \varepsilon_{\sigma_\eta}(x) \rangle$ and max $[\varepsilon_{\sigma_\eta}(x)]$ as a function of $T_s$ for different stream powers (different colors).

We stress that $\varepsilon_{\sigma_\eta}$ is a metric for the $T_s$-dependent relative error that occurs when the temporal variability of the bed-elevation is evaluated. In Figure 4b, a set of curves $\varepsilon_{\sigma_\eta}(x, T_s)$ evaluated for different $T_s$ (different colors) is reported. As expected, the higher $T_s$ the higher the error, and an error up to 80% occurred for $T_s = 25$.

In order to summarize the curve $\varepsilon_{\sigma_\eta}(x)$ in scalar metrics, we focused (i) on the $T_s$-dependent transect-averaged error; namely $\langle \varepsilon_{\sigma_\eta}(x) \rangle$ and (ii) on the $T_s$-dependent maximum error; i.e., $\max\left[\varepsilon_{\sigma_\eta}(x)\right]$. Figures 4c and 4d report $\langle \varepsilon_{\sigma_\eta}(x) \rangle$ and $\max\left[\varepsilon_{\sigma_\eta}(x)\right]$ as a function of $T_s$. In these charts, one observes that the errors (both mean and maximum) increase with $T_s$. The increment of $T_s$ up to 80 (i.e., $\tilde{T}_s$=320 min) causes a mean error in the estimation of $\sigma_\eta$ of 35% (see Figure 4c) and a maximum error of 150% (see Figure 4d). This means that the error in the measurement of $\sigma_\eta$ may exceed to a great extent the value of $\sigma_\eta$ itself (recall equation (8)). Therefore, the increment of the sampling time is detrimental for the measurement of the bed-elevation variability.

Analogous to the section 3.1, the effect of the experimental conditions was investigated in terms of $\omega$ (i.e., the dimensionless stream power). Figures 4e and 4f report the curves $\langle \varepsilon_{\sigma_\eta} \rangle$ and $\max\left[\varepsilon_{\sigma_\eta}\right]$ as a function of $T_s$ for all the performed runs. It is apparent that an increment of $\omega$ renders the evaluation of $\sigma_\eta$ more sensitive to the coarsening of the survey frequency. In fact, Figure 4e shows that the average error does not exceed $\sim$10% when $\omega$=2.5 (red curve) whereas is more than $\sim$30% when $\omega$=11.7 (blue curve). On the other hand, Figure 4f reveals that the maximum error is well above $\sim$200% when $\omega$=11.7 (blue curve) whereas is limited to $\sim$70% when $\omega$=2.5 (red curve).

## 4. Discussion

We now report some examples of morphological analyses that can be performed when a frequent and spatially accurate survey of the bed-morphology is available. These analyses can greatly help the understanding of braided river dynamics. Moreover, they demonstrate the importance of the high-sampling-frequency experimental procedure previously described.

### 4.1. Location Along the Transect of the Morphological Processes

The first issue concerns the locationing along the transect of the most significant reworking and compensation processes. To this aim, a metric of the reworking that occurs in the plot $x$ during the time interval $[t_{j_1}, t_{j_2}]$ is introduced. This metric is defined as $\hat{R}(x, T_s)$ and reads

$$\hat{R}(x, T_s) = \sum_{j=j_1}^{j_2} \theta(x, T_s) \frac{|\Delta\tilde{\eta}_j(x, T_s)|}{\mathcal{L}}, \quad \theta(x, T_s) = \begin{cases} 1 & \text{if } |\Delta\tilde{\eta}_j(x, T_s)| \geq \tilde{\delta} \\ 0 & \text{if } |\Delta\tilde{\eta}_j(x, T_s)| < \tilde{\delta}. \end{cases} \tag{9}$$

Similarly to the definition of $\mathcal{E}$ in equation (5), the spatial scale $\mathcal{L}$ is introduced to make the elevation change $|\Delta\tilde{\eta}|$ dimensionless. The term $\theta$ is introduced to consider in the summation only the bed-elevation changes that are above the instrument precision. From a physical point of view, $\hat{R}(x, T_s)$ is the cumulative elevation change in a generic plot $x$ between the two instants $t_{j_1}$ and $t_{j_2}$, and quantifies the morphological activity in that plot. Figure 5a reports the metric $\hat{R}(x, T_s)$ along the transect for three values of the sampling time, $T_s$. It stands out that there are three zones where $\hat{R}(x, T_s)$ is greater than zero (highlighted in gray in Figure 5a), independently on the adopted sampling time. These zones are the active channels of the cross section. Let us consider how the curve $\hat{R}(x)$ changes while the sampling time $T_s$ is increased. Consider first channel 3. The location of the zone where $\hat{R}(x) > 0$ does not change. Differently, the amount of reworked sediments (i.e., the actual value of $\hat{R}(x)$) reduces. This behavior is typical of a channel with stable banks, but with a fast-evolving bottom. Channels 1 and 2 show a different behavior. If the survey time is increased, both the width of the area where $\hat{R}(x) > 0$ and the quantity of reworked sediments reduce. This behavior is ascribable to channels where both banks and bottom evolve fast. It follows that surveys with a high frequency (4 min in this particularly case) are (i) always necessary to capture the dynamics of the bottom (and, in turn, they are crucial to determine the sediment budget of the transect); (ii) often necessary to capture the dynamics of channel banks; and (iii) not fundamental to determine macroscopic indexes of the braided morphology, such as the number of channels in the transect.

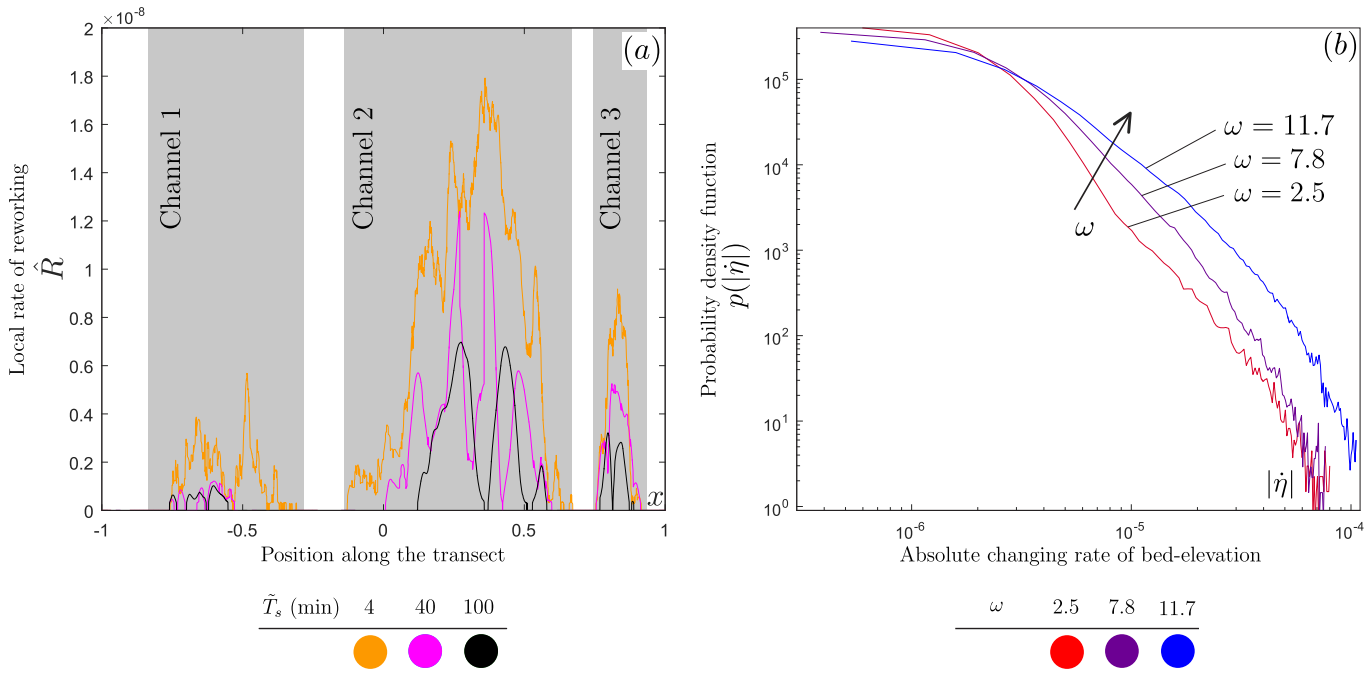


**Figure 5.** (a) Intensity of reworking $\hat{R}(x, T_s)$ (from $\tilde{t}=0$ min to $\tilde{t}=150$ min) along the transect for different sampling times, $T_s$, and for run 6. The gray areas mark the zones of the transect where the three channels were confined during the considered time interval. (b) PDFs of the absolute value of the (dimensionless) changing rate of bed-elevation. Three exemplifying runs with different stream power are reported.

### 4.2. Signature of the Stream Power on the Bed Kinetics of the Transect

The second considered issue is the "signature" that the stream power leaves on the characteristics of bed kinetics. To explore this topic, the absolute changing rate of the bed-elevation is introduced. It is defined as

$$|\dot{\eta}_j(x)| = \theta(x, T_s)\frac{|\Delta\tilde{\eta}_j(x, T_s)|/\mathcal{L}}{\tilde{T}_s/\mathcal{T}}, \quad \theta(x, T_s) = \begin{cases} 1 & \text{if } |\Delta\tilde{\eta}_j(x, T_s)| \geq \tilde{\delta} \\ 0 & \text{if } |\Delta\tilde{\eta}_j(x, T_s)| < \tilde{\delta}, \end{cases} \tag{10}$$

where the sampling time is set to the minimum value (i.e., $\tilde{T}_s=4$ min). The spatial and temporal scales $\mathcal{L}$ and $\mathcal{T}$ are introduced to make the elevation change $|\Delta\tilde{\eta}|$ and the time interval $\tilde{T}_s$ dimensionless, respectively. The term $\theta$ is introduced to consider only the bed-elevation changes that are above the instrument precision. Physically speaking, $|\dot{\eta}_j(x)|$ is a local (at plot $x$) and instantaneous (at time $t_j$) measure of the rate of the morphological activity. The evaluation of $|\dot{\eta}_j(x)|$ at any $x$ and for any $t_j$ leads to a data set that describes the bed kinetics of the braided river in terms of bed-elevation changing rate. This data set encompasses the morphological evolution occurred during the whole run at any plot of the transect. This data set is used to evaluate the PDF (probability density function) of $|\dot{\eta}_j(x)|$. This PDF quantifies the probability of observing a bed-elevation changing rate with a given magnitude.

Insights about braided river dynamics can be gained by comparing the PDFs of $|\dot{\eta}_j(x)|$ obtained from streams with different power, $\omega$ (see Figure 5b, where it should be noted that axes are in logarithmic scale). It stands out that the PDF obtained from the low energy stream (red curve) shows two key characteristics. First, the left peak is high. For $|\dot{\eta}| < 10^{-6}$ the value $p(|\dot{\eta}|)$ given by the red curve is almost double than $p(|\dot{\eta}|)$ given by the blue curve. Second, the right tail is thin. For $|\dot{\eta}| > 2\times10^{-5}$ $p(|\dot{\eta}|)$ corresponding to $\omega=2.5$ is one order of magnitude lower than $p(|\dot{\eta}|)$ corresponding to $\omega=11.7$. This implies that the morphological evolution of the run with $\omega=2.5$ takes place through a greater number of slow morphological alterations. Indeed, events with high rate are quite rare. On the other hand, in the case of the high energy stream (high $\omega$, blue curve) the PDF exhibits a lower left peak and a fatter right tail. This suggests that fast sediment pulses are crucial in determining the bed kinetics in the case $\omega=11.7$. Finally, an intermediate behavior is observed for $\omega=7.8$ (purple curve).

### 4.3. Implication for Field Surveys

The last considered issue concerns the application of the results reported in section 3 for the interpretation of field surveys of real rivers (e.g., performed with GPS, LiDAR, or photogrammetric techniques). To this aim, the first step is to find a time scale that is suitable for extending the results from the river model to a real river. This is a hard task, since no validated theories exist yet for this purpose [e.g., *Sapozhnikov and Foufoula-Georgiou*, 1997]. To our knowledge, only *Lindsay and Ashmore* [2002] tackled this issue. They focused on the Sunwapta River (Alberta, Canada). The mean (maximum) discharge is about 5 (10) $m^3\ s^{-1}$, whereas the mean sediment diameter is of the order of 30 mm. The laboratory analyses were performed in a flume model with a constant discharge of 1.5 $L\ s^{-1}$, a mean sediment diameter $\tilde{d}_{50}=0.7$ mm, and a stream power $\omega=6.4$ (see also run 10 in Table 1). They found that the flume model evolution was about 30 times faster than the real river dynamics.

Our results demonstrated that the maximum time interval between two consecutive surveys should not exceed 4–8 min, in order to capture all the relevant morphological processes. It should be noted that the run by *Lindsay and Ashmore* [2002] was very similar to the runs we performed in this study. It follows that in the real river considered by *Lindsay and Ashmore* [2002], the optimal survey time interval should be $30 \times (4–8) = 120–240$ min. If a longer sampling time is adopted in field measurements, the procedure reported in the supporting information may be used to assess the errors in the measurement process.

## 5. Conclusions

We have assessed the errors that affect the measurement of the time-dependent topography of braided networks in flume experiments. These errors are induced by compensation processes that occur during the time interval that passes between two consecutive surveys of the bed topography. To do this, we adopted a novel experimental technique that allowed us the detailed measurement of the bed-elevation of a flume transect with a minimum time between consecutive surveys equal to 4 min. We emphasize that such a short sampling time was possible because the measurement of the bed-elevation did not require the water discharge to be stopped. Twelve runs were performed, so that the dimensionless stream power, $\omega$, was varied in the range [2–12]. For these values of $\omega$ and at the flume scale, it was found that (i) the coarsening of the survey frequency (increment of $T_s$) induced a strong bias on the eroded/deposited volumes and rates (in agreement with the results of *Lindsay and Ashmore* [2002]) and on the standard deviation of the bed-elevation; (ii) a sampling time in the interval $\tilde{T}_s=4-8$ min seems to be sufficient to capture all the fundamental morphological dynamics that take place at the transect scale, and (iii) the errors occurring for $\tilde{T}_s > 4$ min are significantly related with the dimensionless stream power $\omega$. The results reported in section 3 can be useful to estimate the order of magnitude of the errors that affect the measurements (both at the lab-scale and in field studies) when surveys are not performed with the optimal survey frequency.

**Acknowledgments**

All data reported in this work are given in tabulated form in the supporting information. Any additional data not reported are available upon request from the corresponding author. We thank Matteo Buschini, Jan Sabbagh, and Gianluca Siddi for their precious help in running the experiments. Three anonymous reviewers and the Associated Editor are also acknowledged for their help in increasing the readability of our work and stimulating the discussion about the use of our results.

## References

Anderson, S., and J. Pitlick (2014), Using repeat LiDAR to estimate sediment transport in a steep stream, *J. Geophys. Res. Earth Surf.*, *119*, 621–643, doi:10.1002/2013JF002933.

Ashmore, P. (1982), Laboratory modelling of gravel braided river morphology, *Earth Surf. Processes Landforms*, *7*(3), 201–225.

Ashmore, P. (1991), How do gravel-bed rivers braid?, *Can. J. Earth Sci.*, *28*(3), 326–341.

Ashmore, P. (1993), Anabranch confluence kinetics and sedimentation processes in gravel-braided streams, *Geol. Soc. Spec. Publ.*, *75*, 129–146.

Ashmore, P. (2013), Morphology and dynamics of braided rivers, in *Treatise on Geomorphology*, edited by J. Shroder and E. Wohl, vol. 9, pp. 289–312, Elsevier, Academic, San Diego, Calif., doi:10.1016/S1099-4831(10)06803-3.

Ashmore, P., and G. Parker (1983), Confluence scour in coarse braided streams, *Water Resour. Res.*, *19*(2), 392–402.

Ashmore, P., W. Bertoldi, and J. Tobias Gardner (2011), Active width of gravel-bed braided rivers, *Earth Surf. Processes Landforms*, *36*(11), 1510–1521.

Ashworth, P. (1996), Mid-channel bar growth and its relationship to local flow strength and direction, *Earth Surf. Processes Landforms*, *21*(2), 103–123.

Bertoldi, W. (2012), Life of a bifurcation in a gravel-bed braided river, *Earth Surf. Processes Landforms*, *37*(12), 1327–1336.

Bertoldi, W., and M. Tubino (2005), Bed and bank evolution of bifurcating channels, *Water Resour. Res.*, *41*, W07001, doi:10.1029/2004WR003333.

Bertoldi, W., L. Zanoni, and M. Tubino (2009a), Planform dynamics of braided streams, *Earth Surf. Processes Landforms*, *34*(4), 547–557.

Bertoldi, W., P. Ashmore, and M. Tubino (2009b), A method for estimating the mean bed load flux in braided rivers, *Geomorphology*, *103*(3), 330–340.

Bertoldi, W., N. Drake, and A. Gurnell (2011), Interactions between river flows and colonizing vegetation on a braided river: Exploring spatial and temporal dynamics in riparian vegetation cover using satellite data, *Earth Surf. Processes Landforms*, *36*(11), 1474–1486.

Bertoldi, W., M. Welber, A. Gurnell, L. Mao, F. Comiti, and M. Tal (2015), Physical modelling of the combined effect of vegetation and wood on river morphology, *Geomorphology*, *246*, 178–187.
Beschta, R., and W. Ripple (2012), The role of large predators in maintaining riparian plant communities and river morphology, *Geomorphology*, *157–158*, 88–98.
Brasington, J., B. T. Rumsby, and R. A. McVey (2000), Monitoring and modelling morphological change in a braided gravel-bed river using high resolution GPS-based survey, *Earth Surf. Processes Landforms*, *25*(9), 973–990.
Brasington, J., J. Langham, and B. Rumsby (2003), Methodological sensitivity of morphometric estimates of coarse fluvial sediment transport, *Geomorphology*, *53*(3–4), 299–316.
Bristow, C., and J. Best (1993), Braided rivers: Perspectives and problems, *Geol. Soc. Spec. Publ.*, *75*, 1–11.
Casas, A., S. Lane, D. Yu, and G. Benito (2010), A method for parameterising roughness and topographic sub-grid scale effects in hydraulic modelling from LiDAR data, *Hydrol. Earth Syst. Sci.*, *14*(8), 1567–1579.
East, A., et al. (2015), Large-scale dam removal on the Elwha River, Washington, USA: River channel and floodplain geomorphic change, *Geomorphology*, *228*, 765–786.
East, A., K. Jenkins, P. Happe, J. Bountry, T. Beechie, M. Mastin, J. Sankey, and T. Randle (2016), Channel-planform evolution in four rivers of Olympic National Park, Washington, USA: The roles of physical drivers and trophic cascades, *Earth Surf. Processes Landforms*, *42*, 1011–1032.
Egozi, R., and P. Ashmore (2008), Defining and measuring braiding intensity, *Earth Surf. Processes Landforms*, *33*(14), 2121–2138.
Federici, B., and C. Paola (2003), Dynamics of channel bifurcations in noncohesive sediments, *Water Resour. Res.*, *39*(6), 1162, doi:10.1029/2002WR001434.
Fuller, I., A. Large, M. Charlton, G. Heritage, and D. Milan (2003), Reach-scale sediment transfers: An evaluation of two morphological budgeting approaches, *Earth Surf. Processes Landforms*, *28*(8), 889–903.
Gran, K., and C. Paola (2001), Riparian vegetation controls on braided stream dynamics, *Water Resour. Res.*, *37*(12), 3275–3283.
Hicks, D., M. Duncan, S. Lane, M. Tal, and R. Westaway (2007), 21 contemporary morphological change in braided gravel-bed rivers: New developments from field and laboratory studies, with particular reference to the influence of riparian vegetation, *Dev. Earth Surf. Processes*, *11*, 557–584.
Jähnig, S., S. Brunzel, S. Gacek, A. Lorenz, and D. Hering (2009), Effects of re-braiding measures on hydromorphology, floodplain vegetation, ground beetles and benthic invertebrates in mountain rivers, *J. Appl. Ecol.*, *46*(2), 406–416.
Jang, C.-L., and Y. Shimizu (2007), Numerical analysis of braided rivers and alluvial fan deltas, *Eng. App. Comp. Fluid*, *1*(1), 15–24.
Jaquette, C., E. Wohl, and D. Cooper (2005), Establishing a context for river rehabilitation, North Fork Gunnison River, Colorado, *Environ. Manage.*, *35*(5), 593–606.
Lane, S. (2000), The measurement of river channel morphology using digital photogrammetry, *Photogramm. Rec.*, *16*(96), 937–961.
Lindsay, J., and P. Ashmore (2002), The effects of survey frequency on estimates of scour and fill in a braided river model, *Earth Surf. Processes Landforms*, *27*(1), 27–43.
Martin, Y., and M. Church (1995), Bedmaterial transport estimated from channel surveys: Vedder River, British Columbia, *Earth Surf. Processes Landforms*, *20*(4), 347–361.
McLean, D., M. Church, and B. Tassone (1999), Sediment transport along lower Fraser River: 1. Measurements and hydraulic computations, *Water Resour. Res.*, *35*(8), 2533–2548.
Milan, D., G. Heritage, and D. Hetherington (2007), Application of a 3D laser scanner in the assessment of erosion and deposition volumes and channel change in a proglacial river, *Earth Surf. Processes Landforms*, *32*(11), 1657–1674.
Mosley, M. (1982), Analysis of the effect of changing discharge on channel morphology and instream uses in a braided river, Ohau River, New Zealand, *Water Resour. Res.*, *18*(4), 800–812.
Murray, A., and C. Paola (1994), A cellular model of braided rivers, *Nature*, *371*(6492), 54–57.
Nicholas, A. (2000), Modelling bedload yield braided gravel bed rivers, *Geomorphology*, *36*(1–2), 89–106.
Paola, C. (1996), Incoherent structures: Turbulence as a metaphor for stream braiding, in *Coherent Flow Structures in Open Channels*, edited by P. Ashworth et al., pp 705–723, John Wiley, Chichester, U. K.
Parker, G., P. Wilcock, C. Paola, W. Dietrich, and J. Pitlick (2007), Physical basis for quasi-universal relations describing bankfull hydraulic geometry of single-thread gravel bed rivers, *J. Geophys. Res.*, *112*, F04005, doi:10.1029/2006JF000549.
Piégay, H., G. Grant, F. Nakamura, and N. Trustrum (2009), Braided river management: From assessment of river behaviour to improved sustainable development, in *Braided Rivers*, pp. 257–275, Blackwell, Oxford, U. K.
Redolfi, M., M. Tubino, W. Bertoldi, and J. Brasington (2016), Analysis of reach-scale elevation distribution in braided rivers: Definition of a new morphologic indicator and estimation of mean quantities, *Water Resour. Res.*, *52*, 5951–5970, doi:10.1002/2015WR017918.
Richards, K., J. Brasington, and F. Hughes (2002), Geomorphic dynamics of floodplains: Ecological implications and a potential modelling strategy, *Freshwater. Biol.*, *47*(4), 559–579.
Roach, C., M. Shoulders, and R. Carlson (2005), Conversion of braided streams to stable single thread channels—A discussion of design principles, applications, benefits, and limitations, in *Proceedings of the 2005 World Water and Environmental Resources Congress: Impacts of Global Climate Change*, pp. 570, American Society of Civil Engineers (ASCE ), Reston, Va.
Rohde, S., F. Kienast, and M. Brgi (2004), Assessing the restoration success of river widenings: A landscape approach, *Environ. Manage.*, *34*(4), 574–589.
Sapozhnikov, V., and E. Foufoula-Georgiou (1997), Experimental evidence of dynamic scaling and indications of self-organized criticality in braided rivers, *Water Resour. Res.*, *33*(8), 1983–1991.
Tal, M., and C. Paola (2007), Dynamic single-thread channels maintained by the interaction of flow and vegetation, *Geology*, *35*(4), 347–350.
Van Der Nat, D., K. Tockner, P. Edwards, J. Ward, and A. Gurnell (2003), Habitat change in braided flood plains (Tagliamento, NE-Italy), *Freshwater Biol.*, *48*(10), 1799–1812.
Vesipa, R., C. Camporeale, and L. Ridolfi (2015), Noise-driven cooperative dynamics between vegetation and topography in riparian zones, *Geophys. Res. Lett.*, *42*, 8021–8030, doi:10.1002/2015GL065688.
Visconti, F., C. Camporeale, and L. Ridolfi (2010), Role of discharge variability on pseudomeandering channel morphodynamics: Results from laboratory experiments, *J. Geophys. Res.*, *115*, F04042, doi:10.1029/2010JF001742.
Visconti, F., L. Stefanon, C. Camporeale, F. Susin, L. Ridolfi, and S. Lanzoni (2012), Bed evolution measurement with flowing water in morphodynamics experiments, *Earth Surf. Processes Landforms*, *37*(8), 818–827.
Westaway, R., S. Lane, and D. Hicks (2003), Remote survey of large-scale braided, gravel-bed rivers using digital photogrammetry and image analysis, *Int. J. Remote Sens.*, *24*(4), 795–815.

Wheaton, J., J. Brasington, S. Darby, and D. Sear (2010), Accounting for uncertainty in DEMs from repeat topographic surveys: Improved sediment budgets, *Earth Surf. Processes Landforms*, *35*(2), 136–156.

Williams, R., J. Brasington, D. Vericat, and D. Hicks (2014), Hyperscale terrain modelling of braided rivers: Fusing mobile terrestrial laser scanning and optical bathymetric mapping, *Earth Surf. Processes Landforms*, *39*(2), 167–183.

Williams, R. D., C. D. Rennie, J. Brasington, D. M. Hicks, and D. Vericat (2015), Linking the spatial distribution of bed load transport to morphological change during high-flow events in a shallow braided river, *J. Geophys. Res. Earth Surf.*, *120*, 604–622, doi:10.1002/2014JF003346.